

Hybrid Learning of Vessel Segmentation in Retinal Images

Worapan Kusakunniran¹, Peeraphat Charoenpanich², Perapat Samunyanoraset³, Sarocha Suksai⁴, Sarattha Kanchanapreechakorn⁵, Qiang Wu⁶ and Jian Zhang⁷

ABSTRACT: In this paper, a novel technique of vessel segmentation in retinal images using a hybrid learning based approach is proposed. Unlike most other existing methods, a double-layer segmentation technique combining supervised and instance learning steps is introduced to enhance a sensitivity score of segmenting retinal blood vessels. The supervised learning based approach alone may not cope with unseen patterns caused by intrinsic variations in shapes, sizes, and color intensities of blood vessels across different retinal images. Thus, in the proposed hybrid learning solution, the supervised learning part is adopted to compute initial seeds of segmented vessels. They are then fed into the instance learning part as an initial foreground to further learn specific characteristics of vessels in each individual image. In the supervised learning step, the support vector machine (SVM) is applied on three types of features including green intensity, line operators, and Gabor filters. An iterative graph cut is adopted in the instance learning step, together with the pre-processing of morphological operations and the watershed algorithm. The proposed method is evaluated using two well-known datasets, DRIVE and STARE. It shows promising sensitivity scores of 82.6% and 82.0% on the DRIVE and STARE datasets respectively, and outperforms other existing methods in the literature.

Keywords: Vessel Segmentation, Retinal Image, Hybrid Learning, Supervised Learning, Instance Learning

DOI: 10.37936/ecti-cit.2021151.240050

Received March 14, 2020; revised May 15, 2020; accepted June 1, 2020; available online November 18, 2020

1. INTRODUCTION

This paper focuses on developing a technique for segmentation of blood vessels in retinal images. Segmentation results of blood vessels can be further used in many analysis tasks for detecting abnormalities of vessels, including a severe stage of diabetic retinopathy. Thus, it is important to have the technique for segmenting retinal vessels in an automatic way with good performance. Several related methods have been proposed to address this challenge [1]. The existing techniques of vessel segmentation can be classified into two groups, instance-learning and supervised-learning based approaches.

A key challenge of retinal blood vessels segmenta-

tion is dealing with variations in shapes, scales, sizes, and colors of the vessels themselves. Across different retinal images, pixels' intensities of blood vessels may vary significantly. Even within an individual image, shapes and sizes of vessels can have different locations and types (e.g arteries and veins). This is especially true for retinal images with signals of a disease. For example, severe non-proliferative and proliferative stages of diabetic retinopathy contain abnormalities of blood vessels. Thus, variations of retinal blood vessels could be very significant.

Starting with instance learning based approaches, the main difficulty is that preset parameters cannot cope well with different characteristics in different

¹Faculty of Information and Communication Technology, Mahidol University, Thailand, E-mail: worapan.kun@mahidol.edu (Corresponding author)

^{2,3,4,5}Faculty of Information and Communication Technology, Mahidol University, Thailand, E-mail: p.peeraphat@outlook.com, perapat1972@gmail.com, sarocha.suks@gmail.com and j.sarattha@gmail.com

^{6,7}School of Electrical and Data Engineering, University of Technology Sydney, Australia, E-mail: qiang.wu@uts.edu.au and jian.zhang@uts.edu.au

retinal images. For supervised learning based approaches, the learned segmentation model does not work efficiently with unseen vessels' characteristics caused by variations mentioned above.

Lately, CNN-based approaches, which also belong to the category of supervised learning, have been proposed. However, they cannot surpass the limited performance of sensitivity scores, since they need more training data to address variations of blood vessels. This paper, therefore, proposes a hybrid learning solution to overcome the limitations of each learning category.

Examples of instance learning and supervised learning (including CNN) based approaches of the retinal blood vessels segmentation are reviewed below, to demonstrate how they are developed and work in different perspectives.

Using instance-learning, for example, the paper [2] began with extracting image ridges. They were later grouped into sets of primitives to approximately form up straight-line elements which were parts of vessels. The paper [3] used pixels' intensities with vessel enhancement as features. Then, the vessel segmentation was performed using a Self-Organizing Map (SOM) with Otsu's method to estimate the neuron class in a neural network as an unsupervised clustering method. The proposed method in [4] used Heidelberg Retina Tomograph (HRT) images. They contained typical double-edged shapes of retinal vessels with different qualities. The reconstruction of vascular structures in retinal images was done on the green channel with the two-stage approach. A dedicated detector was applied for certain widths of the vessels. In addition, the Gaussian function was used for helping to detect the center line of vessels. Then, an unbiased detector of curvilinear structures was applied to detect vessels.

In [5], histogram equalization was used to enhance the contrast in the retinal image. The distance transform algorithm was then applied to create a distance map image to calculate the directions and the magnitudes of the vessels' gradients. These pieces of information were used to construct the graph. Then, the graph cut algorithm was applied to segment the graph into vessel and non-vessel parts.

The techniques in this first category have a key advantage of not requiring a training process and a large set of labeled data for training. However, they are fairly sensitive to the intra-variations among the retinal images, which may include variations in color tones and intensities of vessels.

The group of supervised-learning based approaches is described next. For example, [6] used basic and orthogonal line operators and the green channel as features, without any pre-processing or enhancement applied on the input image. This was done to preserve the vessel structure before further analysis. The line operators were calculated at twelve different angles. Also, vessels and backgrounds had more contrast in

the green channel, when compared with the red and blue channels. Then, an SVM was used as the final classification tool. [7] used seven features extracted based on the inverted green channel, Gabor Wavelet, and line operator. Similarly, the Bayesian network and SVM were attempted as the classification tools.

In addition, cellular neural networks with line detection on the inverted green channel were used for the segmentation in [8]. They avoided the problems of noise and low contrast between vessels and backgrounds. The proposed method in [9] extracted features based on local area shape-based features combined with multi-scale local statistical features from the green channel. Three types of morphological operators were applied. First, the opening operation was applied to remove smaller bright details such as noise points or pathological areas. Second, the closing operation was employed to enhance dark details which mainly contained vessels. Third, the difference between erosion and dilation was used to enhance the edge information. An SVM was used to find the optimal hyperplane for segmenting vessels from backgrounds.

In [10], they applied adaptive histogram equalization and morphological operations in the pre-processing stage. Then the local binary pattern and the gray level co-occurrence matrix were applied on the pre-processed image. For the feature extraction, the energy, contrast, correlation, and homogeneity were used. An SVM was also used in this paper for the vessel classification. In [11], 7D feature vectors from the gray-level-based features and the moment invariants-based features were computed. Then, a neural network was used as the pixel-based classification tool. It also included two post-processing steps, which were filling of pixel-gaps and removing false detections.

More recently, several methods using convolutional neural networks (CNN) have been proposed for solving the segmentation problem of vessels in retinal images. Their techniques are all very similar, relying on CNN, but with varieties of CNN architectures. In [12], a deformable U-Net is adopted, where deformable convolutional layers are added into the conventional neural networks. This could address the challenges of high-variations of shapes and scales of blood vessels. While in [13], U-Net and Dense-Net structures are combined and used to construct the segmentation model. Rotation and image mirroring are adopted in the data augmentation process, and the CLAHE algorithm is applied for the pre-processing. In [14], dense U-Net is used under an assumption that retinal vessels are tiny, which means they could be learned effectively using a patch-based learning strategy.

In [15], an encoder-decoder architecture is adopted into a fully convolutional deep neural network, using dilated spatial pyramid pooling with multiple dilation

rates. In [16], an encoder-decoder based octave convolution network is introduced for addressing the vessels' segmentation challenges of variations in sizes and shapes. Also, in [17], a convolutional neural network with a multi-scale residual is adopted to solve the scale-variation of retinal vessels. In [18], five different models of deep convolutional neural networks are attempted using high-resolution patches. M-AlexNet provides the best segmentation result. The main limitation of CNN based methods is they require many computational resources and a sufficiently large set of labeled data for training the segmentation model. Also, as mentioned in the experimental comparisons of this paper, they could achieve high specificity values, but sensitivity scores were not high enough.

One challenge for techniques in this second category could be the overfitting problem, especially when there are not enough training data samples. This occurs often for the case of medical image analysis, where it is difficult to obtain a large number of medical images with related groundtruth. As a result, many small vessels could be missed from the segmentation. Moreover, the main advantage of this category is that well-trained model can be used directly without any additional learning steps or calculations.

Therefore, in this paper, a hybrid solution combining good aspects of both instance-learning and supervised-learning concepts is proposed to solve the problem of segmentation of vessels in retinal images. The supervised-learning using SVM learns pixels of blood vessels based on features of green intensity, line operators, and Gabor filters. The color transfer technique is also adopted to normalize color tones of retinal images before using them in the SVM learning process. Then, the detected vessel-pixels with high confidence values are used as the initial seeds to be learned in the instance learning using a graph cut. This extends the segmentation results to cover remaining blood vessels in the retinal image, especially small branches of the vessels. The proposed method was validated on two well-known datasets, namely DRIVE and STARE. It achieved outstanding sensitivity performance when compared with the other methods in the literature.

Motivations for adopting each technique in the proposed method are explained in this paragraph. The SVM is applied in this paper as the classification tool because it focuses on producing a single binary output of vessel and non-vessel. It also contains a small number of hyper-parameters and guarantees a global optimum [19]. In addition, the color transfer technique is adopted in this paper to normalize color tones of retinal images. This is important to reduce variations of retinal blood vessels for a learning process in the supervised learning step. Also, this makes it easier for the instance learning step to extend coverage areas of blood vessels. The Gabor filter is used to detect key vessel features because it can describe

vessel textures/patterns in various scales and orientations. Moreover, the iterative graph cut is used as a main tool in the instance learning step, due to its flexibility and ability to capture multiple characteristics of vessels within individual retinal images.

The rest of this paper is organized as follows. The details of the proposed method are explained in section 2. The experimental results and discussions are summarized in section 3. Finally, the conclusion is drawn in section 4.

2. PROPOSED METHOD

Figure 1 shows an overview of the framework of the proposed method hybridizing supervised and instance learning approaches for the coarse-level and fine-level segmentation of vessels in retinal images. In the pre-processing stage, the green channel is split and used in the further processes because it gives the best contrast between vessels and background, when compared with other two channels of red and blue. Then, the histogram equalization is applied to enhance the contrast. It begins with the construction of a color histogram of the green channel ($hist$), with 256 bins.

$$hist = \{h_i\}_{i=0}^{255} \quad (1)$$

Then the accumulative color histogram ($C = \{c_j\}_{j=0}^{255}$) is computed with Eq. 2.

$$c_j = \sum_{i=0}^j h_i \quad (2)$$

The pixel value p_j is then updated using Eq. 3.

$$round\left[\frac{c_j - c_0}{W \times H - c_0}(255)\right] \quad (3)$$

W and H are width and height of the input image respectively, and 255 is the maximum value of the pixel intensity. The sample output of this enhancement process is shown in figure 2.

Next, in the coarse-level segmentation stage, the supervised learning approach is applied to train the extracted high-level features including green intensities, basic-line operators, orthogonal-line operators, and Gabor features, for recognizing vessels. These segmented vessels are used as pre-seeds in the fine-level segmentation stage based on the instance learning approach. The pre-seeds are refined and used as the initial foreground (i.e. vessels) in the iterative graph cut for finalizing the vessel areas. The detailed processes are explained in the following sub-sections.

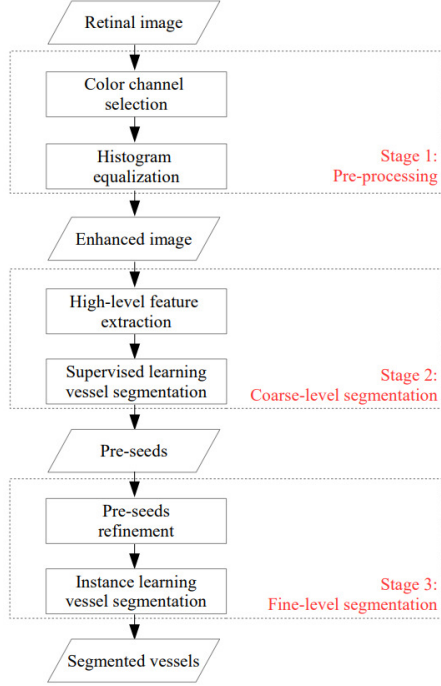


Fig.1: The overview of the proposed method.

2.1 Segmentation Level 1 using Supervised Learning (Coarse-Level Segmentation)

In this level, four types of features are extracted for each pixel in the retinal image. The first feature is the intensity of the green channel since it provides the best contrast information between vessels and background, when compared with the red and blue channels.

Due to the intra-variation of color statistics across different images, the green channels (I_g) of all images are normalized to match the statistic of the reference image (I_R). This process reduces such variation, using the color transfer based-approach [20]. Since this color-statistic normalization process is performed on the single color channel, it can be done on the channel directly without converting the image to the $l\alpha\beta$ color space. The process is defined in Eq. 4.

$$\widetilde{I}_g(p) = (I_g(p) - \mu_g) \frac{\sigma_R}{\sigma_g} + \mu_R \quad (4)$$

$I_g(p)$ is the pixel p of the image I_g . $\widetilde{I}_g(p)$ is the transferred value of $I_g(p)$. μ_g and μ_R are the means of I_g and I_R respectively. σ_g and σ_R are the standard deviations of I_g and I_R respectively. Also, the transferred values must be trimmed up or down into the range of the green channel.

Two more features are extracted using line operators [6,7]. The second feature is computed based on the basic line operator. It is a line with fixed length centered at the considered pixel with 12 orientations spanning 360 degrees, including 0° , 30° , 60° , 90° , 120° , 150° , 180° , 210° , 240° , 270° ,

300° , and 330° . The average gray level of the image is evaluated along lines. This is done in order to find the line direction among the 12 directions noted above that provides the maximum gray level, denoted as $\widetilde{\theta}$. The θ at the pixel of the coordinate (i, j) is calculated with Eq. 5.

$$\widetilde{\theta} = \operatorname{argmax}_\theta \sum_{x=i-k}^{i+k} \widetilde{I}_g(x, q) \quad (5)$$

$\theta \in \{0^\circ, 30^\circ, 60^\circ, 90^\circ, 120^\circ, 150^\circ, 180^\circ, 210^\circ, 240^\circ, 270^\circ, 300^\circ, 330^\circ\}$, $\widetilde{I}_g(x, q)$ is the pixel at the coordinate (x, q) of \widetilde{I}_g , $q = x \tan(\theta) - i \tan(\theta) + j$, and k is a parameter defining the length of the considered line as $2k + 1$.

The next step is to compute the difference by subtracting the mean value of all pixels on the line of the rotation $\widetilde{\theta}$ centered at the coordinate (i, j) with length of $2k + 1$ from the average gray level within the square window with the size of $(2n + 1) \times (2n + 1)$. This difference (S) is called the line strength, and is calculated using Eq. 6,

$$S = \frac{\sum_{x=i-k}^{i+k} \widetilde{I}_g(x, r)}{2k + 1} - \frac{\sum_{a=-n}^n \sum_{b=-n}^n \widetilde{I}_g(i+a, j+b)}{(2n + 1) \times (2n + 1)} \quad (6)$$

where $r = x \tan(\widetilde{\theta}) - i \tan(\widetilde{\theta}) + j$.

The value S is then used to determine whether the considered pixel is a vessel or not. Any pixel with a high value is assumed to be part of a vessel. It will be used as a feature in the supervised learning process. Figure 3 shows the sample output of the basic line operator.

In addition, to improve the segmentation of a pixel that is located on a thin vessel, the third feature is extracted from the orthogonal line operators by evaluating the average gray level of the neighboring pixels along the line that is perpendicular to the second feature. The rotation of the perpendicular line is denoted as $\widetilde{\theta}_o$. Its strength is denoted as S_o . S_o can be obtained by subtracting the mean value of all pixels on the line of the rotation $\widetilde{\theta}_o$ centered at the coordinate (i, j) with the length of $2k + 1$ from the average gray level within the same square window used in the second feature. The calculation uses the same equation (6) above, where $y = x \tan(\widetilde{\theta}_o) - i \tan(\widetilde{\theta}_o) + j$.

The fourth feature is based on the Gabor filter [21-23]. The Gabor filter is a linear filter that has been broadly used for multi-scale and multi-directional edge detection. It can be used to detect oriented features of vessels in the retinal image. It can be fine-tuned for particular scales and directions. The response of a Gabor filter kernel is defined by the product of a function f and a complex sinusoid, using Eq. 7.

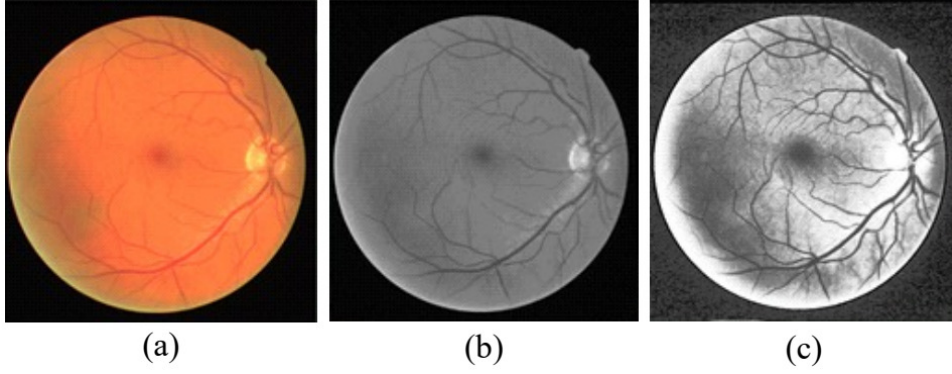


Fig.2: The enhancement on the green channel. (a) An original image. (b) A split green channel image. (c) An applied histogram equalization of (b).

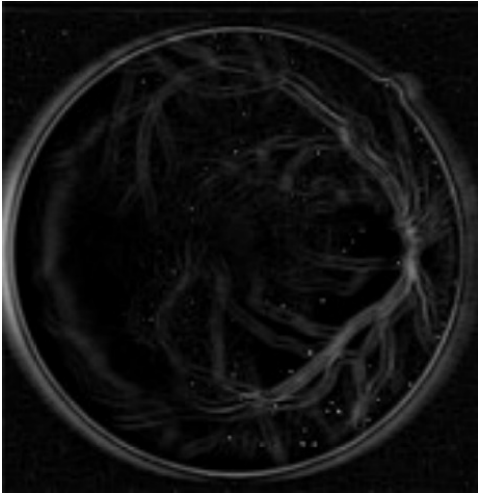


Fig.3: The sample output of the basic line operator.

$$f(x, y, \theta, \lambda) = e^{-\frac{x^2 + \gamma^2 y^2}{2\sigma^2}} e^{i(2\pi \frac{x}{\lambda} + \psi)} \quad (7)$$

$\hat{x} = x\cos(\theta) + y\sin(\theta)$, $\hat{y} = -x\sin(\theta) + y\cos(\theta)$, θ is the orientation, σ is the scale, λ is the wavelength of the sinusoidal factor, γ is the spatial aspect ratio, and ψ is the phase offset of the sinusoidal factor.

In this paper, the Gabor filter is applied to the inverted green channel of the retinal image, using a 2D convolution operator. The maximum Gabor response across the orientation (θ) spanning from 0 to π degrees in steps of $\pi/18$, is calculated for each pixel at four different scales (σ) of 2, 3, 4 and 5. Then the maximum response $f_s(x, y, \theta, \lambda_s)$ across the orientation at each scale λ_s is taken as the pixel feature using Eq. 8.

$$f_s(x, y, \theta, \lambda_s) = \max_{\theta \in \{0, \frac{\pi}{18}, \frac{2\pi}{18}, \dots, \pi\}} f_s(x, y, \theta, \lambda_s) \quad (8)$$

In this stage of the coarse-level segmentation of vessels in the retinal image, a Support Vector Machine (SVM) [24-28] is used as the supervised classifier for the pixel classification. In the classification

process, each pixel of the retinal image is placed into one of two label classes, vessel and non-vessel, which can be separated into the two classes of samples with the best generalization. In the training phase using SVM to build up the vessel classification model, sample positive (i.e. vessel) and negative (i.e. non-vessel) pixels are taken from the groundtruth images with the 4 types of extracted feature vectors as explained above.

When using SVM [24-28] in the training phase of this binary classification problem, labeled training data $\{(d_m, c_m)\}_{m=1}^M$ is required, where m is the total number of training samples. The training dataset needs both positive samples where d_m is the extracted feature vector of the vessel pixel and the class label c_m is represented by +1, and negative samples where d_m is the extracted feature vector of the non-vessel pixel and the class label c_m is represented by -1.

In this paper, the SVM solves the hyperplane for the two-class ($c_m = +1, c_m = -1$) classification problem by using the optimization in Eq. 9.

$$\min_{w, b, \xi} \quad \frac{1}{2} w^T w + C \sum_{m=1}^M \xi_m \quad (9)$$

$$\text{subject to} \quad c_m (w^T \phi(d_m) + b) \geq 1 - \xi_m$$

$\xi_m \geq 0$ is the margin width, w is a weight vector, b is a bias parameter, $\phi(d_m)$ is the kernel mapping for a higher-dimensional space, and $C \geq 0$ is the regularization parameter. In this paper, the histogram intersection is used as the kernel. Eq. 9 is then determined with the dual optimization in Eq. 10.

$$\min_{\alpha} \quad \frac{1}{2} \alpha^T Q \alpha - I \alpha \quad (10)$$

$$\text{subject to} \quad c^T \alpha = 0$$

$0 \leq \alpha \leq C$, I is the all-one vector of size M , Q is the $M \times M$ positive-value matrix, $Q_{i,j} = c_i c_j K(d_i, d_j)$, $K(d_i, d_j) = \phi(d_i)^T \phi(d_j)$, and $c = [c_m]_{m=1}^M$. Next, the

optimal w is solved with Eq. 11.

$$w = \sum_{m=1}^M c_m \alpha_m \phi(d_m) \quad (11)$$

The final decision function is defined in Eq. 12 for the given input feature vector d_{in} .

$$f(w^T \phi(d_{in}) + b) = f\left(\sum_{m=1}^M c_m \alpha_m K(d_m, d_{in}) + b\right) \quad (12)$$

$f(x)$ returns +1 for the vessel class if $f(x) \geq 0$. Otherwise, $f(x)$ returns -1 for the non-vessel class.

The trained model is then used to classify pixels in the retinal image into vessel and non-vessel pixels with equation (12). The vessel pixels with the high confidence values in the top 25% percentiles are used as pre-seeds for the next stage of instance-based learning.

2.2 Segmentation Level 2 using Instance Learning (Fine-Level Segmentation)

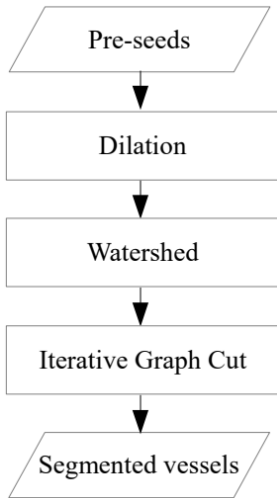


Fig.4: The overall framework of the proposed fine-level segmentation.

Figure 4 shows the overall framework of the proposed fine-level segmentation. This level of segmentation uses the pre-seeds of vessels computed in the previous level of segmentation as the initial input. First, the pre-seeds are refined using morphological operations [29, 30]. Dilation is applied on the pre-seeds to enlarge candidate areas of vessels, which will be refined at the end of this process using the iterative graph cut. The dilation factor is set to be 3, with a disk-shaped structuring element having radius = 3. The sample result is shown in Figure 5.



Fig.5: Dilation applied on the pre-seed image.

Then the watershed algorithm [31] is applied to reduce the noise from the pre-seeds. The output from the watershed is then used as the initial foreground (i.e. vessels) in the iterative graph cut algorithm [32]. The existing usages of graph cut based their approaches [33-36] on the initialization of a bounding box or region covering the target object. However, our method uses the pre-seed pixels obtained from the coarse-level segmentation based on supervised learning as the known foreground pixels for building up the initial foreground model using Gaussian Mixture Models (GMMs).

The graph is first constructed where each node represents each pixel in the image. There are two additional special nodes, including the source node representing foreground or vessels, and the sink node representing background or non-vessels. Each node in the graph is then connected to neighboring nodes and the two special nodes.

The weight of the link connecting each node to the source node is computed using the foreground Gaussian mixture model. The weight of the link connecting each node to the sink node is computed using the background Gaussian mixture model. Then the weight w_{p_1, p_2} of the link connecting between two nodes of two pixels (p_1, p_2) is computed using the linked pixels' similarity, using equation 13 [37,38].

$$w_{p_1, p_2} = \frac{50}{dist(p_1, p_2)} \exp^{-\beta \|pv_1 - pv_2\|^2} \quad (13)$$

$dist(p_1, p_2)$ is the distance between the pixels p_1 and

p_2 coordinates, pv_1 and pv_2 are the pixel intensities of the pixels p_1 and p_2 respectively, $\beta = \frac{1}{2\langle (pv_1 - pv_2)^2 \rangle}$, and $\langle . \rangle$ denotes the expectation over the image sample. The constant value of 50 is used in the equation since it is the value suggested for the segmentation task in [39] for model calculations.

The models are initially created based on the refined pre-seeds. Then the updated foreground and background pixels are used for constructing the models in the next iteration. In each iteration of the iterative graph cut, the mincut algorithm [40, 41] is used to cut the graph into two segments with the minimum cutting cost. The cost function is the summation of weights of the links being cut.

The pixels on the nodes connecting to the source node are said to be foreground pixels or vessel pixels. The pixels on the nodes connecting to the sink node are said to be background pixels or non-vessel pixels. All of these processes are iteratively repeated until the segmentation converges or the maximum number of iterations is reached.

In the final step, post-processing is applied on the segmented image. The morphological operations are then applied again to fill holes in vessels and remove noise. Also, the outer boundary of the retina contour is detected and removed from the final output image.

3. EXPERIMENTS AND DISCUSSIONS

Two public retinal image datasets were used to evaluate the proposed method, the structured analysis of the retina (STARE) dataset [42] and the digital retinal images for vessel extraction (DRIVE) dataset [2]. The STARE dataset consists of 20 digitized images captured by the TopCon TRV-50 fundus camera at 35° field-of-view (FOV), where ten of them present pathology. They are available in the ppm format. The size of each image is 700×605 pixels with eight bits per color channel.

The DRIVE dataset is mainly used to enable comparative studies on blood vessel segmentation in retinal images. It consists of 40 eye-fundus color images acquired by the Canon CR5 nonmydriatic 3CCD camera at 45° field-of-view (FOV), where seven of them present pathology. They are available in the TIF format. The size of each image is 768×584 pixels with eight bits per color channel. For both datasets, 20% of the images were used in the training process, and the remaining 80% of the images were used in the testing phase.

In our experiments, the proposed method was implemented on a computer with Core(TM) i7 CPU@2.70 GHz and 16 GB RAM. It was developed using the library functions of OpenCV in the Microsoft Visual C/C++ environment.

Figure 6 illustrates the sample segmented vessel images using the proposed method. The performance of each method is evaluated based on the sensitivity and the specificity. The sensitivity reflects the ability

of the method to correctly detect vessel pixels, while the specificity presents the ability of the method to correctly detect non-vessel pixels.

The sensitivity is calculated by dividing the true positive with the summation of true positive and false negative. The specificity is calculated by dividing the true negative with the summation of true negative and false positive. The true positive is the number of vessel-pixels that are correctly classified as vessels. The true negative is the number of non-vessel pixels that are correctly classified as non-vessels. The false positive is the number of non-vessel pixels are incorrectly classified as vessels. The false negative is the number of vessel pixels are incorrectly classified as non-vessels.

The ROC curves based on the DRIVE and STARE datasets are shown in figures 7 and 8 respectively. They are computed by varying the confidential score of SVM for classifying vessels and the dilation factor used in the fine-level segmentation step. Tables 1 and 2 provide the results of performance comparisons between our proposed method and the other existing methods in the literature.

As can be seen in tables 1 and 2, our proposed method outperforms the other methods based on the sensitivity values. This is because of the two-level segmentation deployed in our proposed method. The first level using the supervised learning can detect initial seeds of vessel pixels. The performance on different input images can vary because they contain different details of illumination and other signals of disease. The same trained model could not cover all input images with the same performance. The second level using the instance learning began with the segmentation result from the first level and extend the model to cover more foreground pixels based on internal contexts of individual input images.

In addition, the CNN-based approaches [14][15][16][18][43] achieved high specificity scores, but with significantly lower sensitivity scores. This is because in each image, the negative class or non-vessel pixels comprise a significantly higher proportion of the image, when compared to the positive class or vessel pixels. More importantly, the CNN-based approaches belong to the supervised-based learning category which works well on seen data/vessel patterns. However, in fact, retinal vessels contain high variations of shapes, sizes, and colors. So a trained CNN model may not be able to segment vessels that are different from the data seen in the training process. In addition, the complexity of the CNN architecture requires training using a sufficiently large set of labeled data.

Our proposed method addresses these intrinsic variations to some extent, since it uses the instance-based learning technique on pre-seeds of vessels seg-

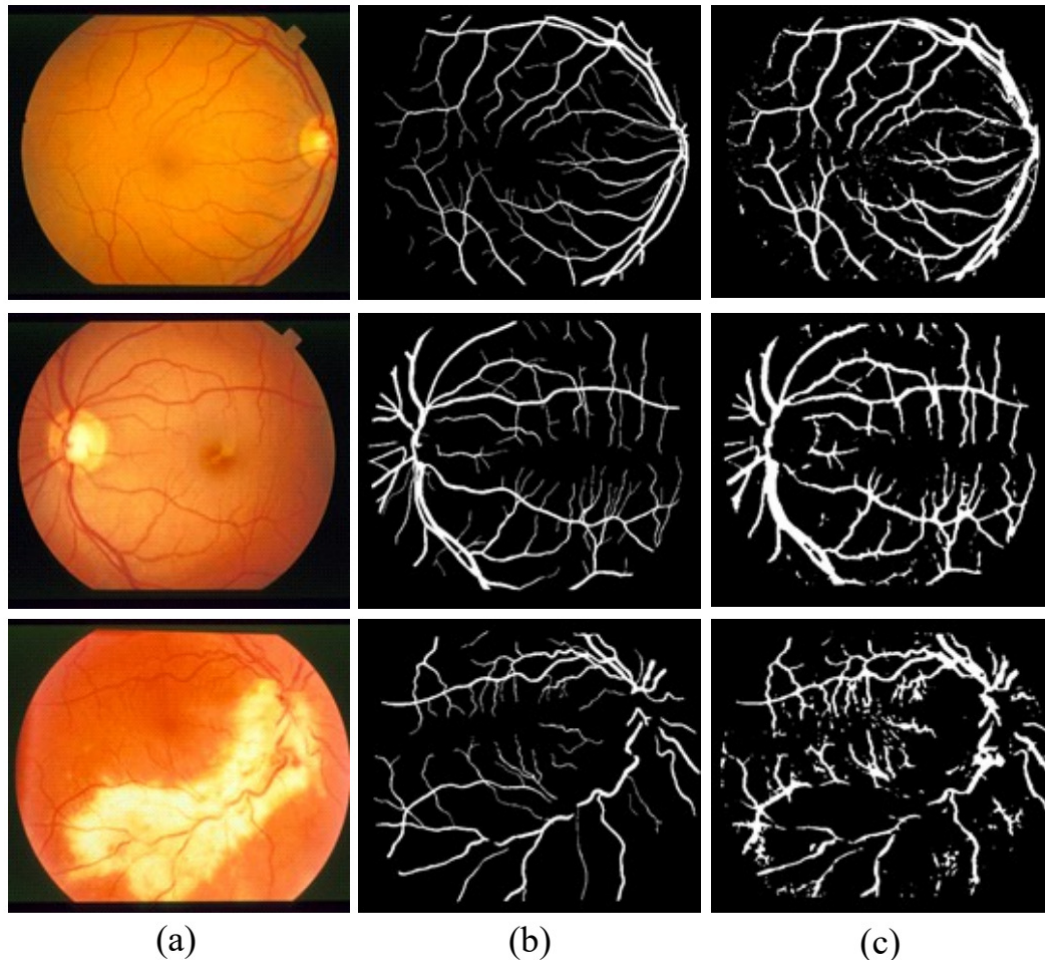


Fig. 6: Sample outputs of the vessel segmentation using the proposed method. (a) Original images. (b) Ground truth images. (c) Segmented images.

mented from the supervised-based learning technique. So our proposed method learns and detect vessels instantly and specifically for individual retinal images. Our proposed method attempts to achieve a high sensitivity because the medical diagnosis commonly needs a high sensitivity [44]. It is important not to miss any parts of the positive class or signals of disease because they are needed to allow a further medical analysis.

Further enhancement of the segmentation performance could be done in the future by filtering and/or clustering the pre-seed values obtained from the first level segmentation. The pre-seed values of vessels could be clustered into multiple groups based on their intensity levels. Then the more reliable pre-seeds could be the cluster(s) containing pixels of approximate connected line(s). The Hough transform could be used to deal with the approximate line detection. This process should improve the pureness of pre-seed values for being used as known vessel pixels, which will lead to better initialization of the graph cut and better segmentation results.

4. CONCLUSION

This paper proposes two-level segmentation of vessels in retinal images. The main contribution of this paper is the development of this hybrid learning solution combining both aspects of instance learning and supervised learning processes. The pair of learning processes could minimize limitations of using either alone, as mentioned in the main content of this paper. The segmented vessels from the supervised learning step are further used as the initial seeds in the instance learning step in order to enhance the sensitivity score. Our method starts with a pre-processing stage using histogram equalization and color transfer. Then the four types of features are extracted and used in the first level of the segmentation: the green intensities, basic-line operators, orthogonal-line operators, and Gabor features. An SVM is used as the vessel classifier. The segmentation output from this level is refined using the second level based on the instance learning approach. It includes morphological operators, watershed, and iterative graph cutting. Our method was validated using two well-known datasets, DRIVE and STARE. Our method achieves outstand-

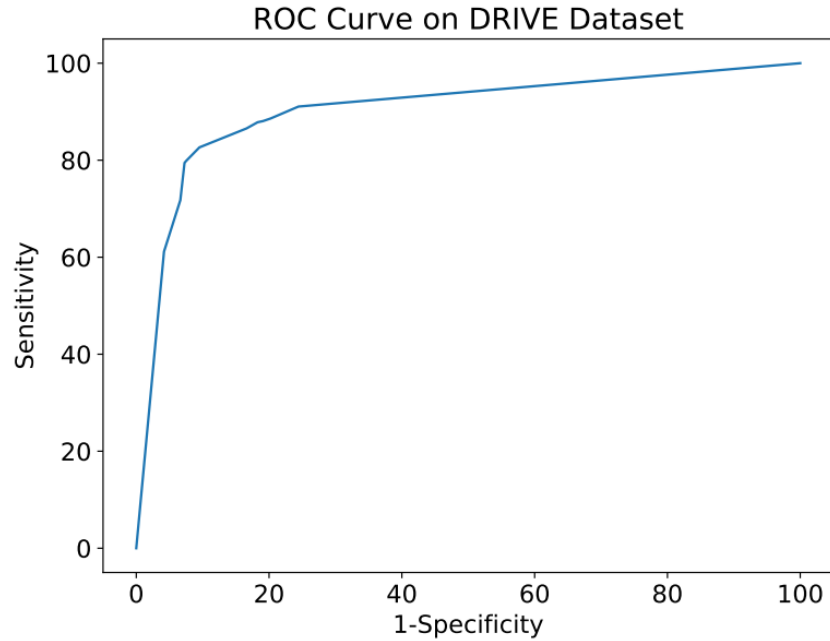


Fig.7: ROC curve on the DRIVE dataset.

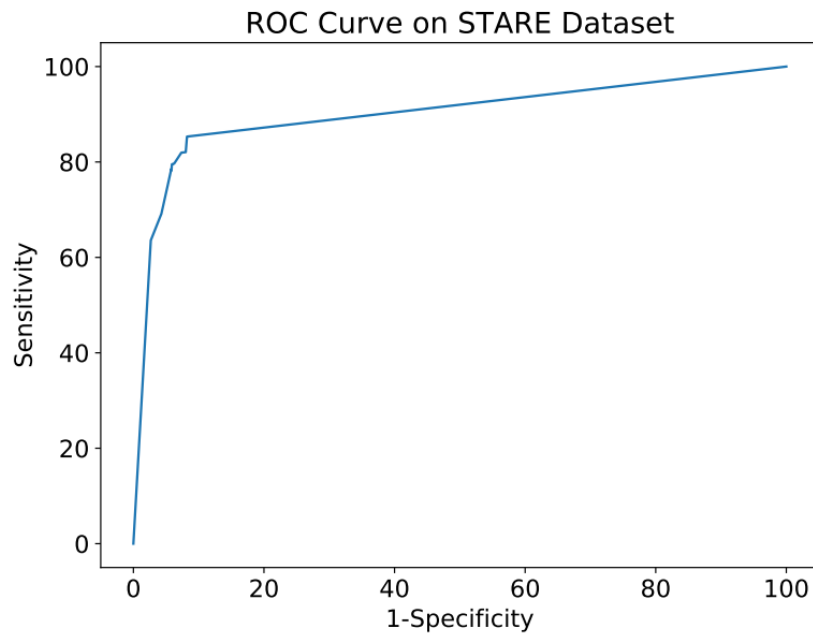


Fig.8: ROC curve on the STARE dataset.

ing sensitivity values, when compared with the other methods in the literature.

References

- [1] A. Imran, J. Li, Y. Pei, J.-J. Yang, and Q. Wang, "Comparative analysis of vessel segmentation techniques in retinal images," *IEEE Access*, vol. 7, pp. 114 862–114 887, 2019.
- [2] J. Staal, M. D. Abràmoff, M. Niemeijer, M. A. Viergever, and B. Van Ginneken, "Ridge-based vessel segmentation in color images of the retina," *IEEE transactions on medical imaging*, vol. 23, no. 4, pp. 501–509, 2004.
- [3] J. Zhang, Y. Cui, W. Jiang, and L. Wang, "Blood vessel segmentation of retinal images based on neural network," in *International Conference on Image and Graphics.*, Springer, 2015, pp. 11–17.
- [4] D. Paulus, S. Chastel, and T. Feldmann, "Vessel segmentation in retinal images," in *Medical Imaging 2005: Physiology, Function, and Structure from Medical Images*, vol. 5746. International Society for Optics and Photonics, 2005, pp. 696–706.

- [5] A. G. Salazar-Gonzalez, D. Kaba, Y. Li, and X. Liu, "Segmentation of the blood vessels and optic disk in retinal images," *IEEE J. Biomedical and Health Informatics*, vol. 18, no. 6, pp. 1874–1886, 2014.
- [6] E. Ricci and R. Perfetti, "Retinal blood vessel segmentation using line operators and support vector classification," *IEEE transactions on medical imaging*, vol. 26, no. 10, pp. 1357–1365, 2007.
- [7] R. Kharghanian and A. Ahmadyfard, "Retinal blood vessel segmentation using gabor wavelet and line operator," *International Journal of Machine Learning and Computing*, vol. 2, no. 5, p. 593, 2012.
- [8] R. Perfetti, E. Ricci, D. Casali, and G. Costantini, "Cellular neural networks with virtual template expansion for retinal vessel segmentation," *IEEE Transactions on Circuits and Systems II: Express Briefs*, vol. 54, no. 2, pp. 141–145, 2007.
- [9] Z. Han, Y. Yin, X. Meng, G. Yang, and X. Yan, "Blood vessel segmentation in pathological retinal image," in *Data Mining Workshop(ICDMW), 2014 IEEE International Conference on.*, IEEE, 2014, pp. 960–967.
- [10] D. S. S. Raja, S. Vasuki, and D. R. Kumar, "Performance analysis of retinal image blood vessel segmentation," *Advanced Computing*, vol. 5, no.2/3, p. 17, 2014.
- [11] D. Marín, A. Aquino, M. E. Gegúndez-Arias, and J. M. Bravo, "A new supervised method for blood vessel segmentation in retinal images by using gray-level and moment invariants-based features," *IEEE transactions on medical imaging*, vol. 30, no. 1, p. 146, 2011.
- [12] Q. Jin, Z. Meng, T. D. Pham, Q. Chen, L. Wei, and R. Su, "Dunet: A deformable network for retinal vessel segmentation," *Knowledge-Based Systems*, vol. 178, pp. 149–162, 2019.
- [13] D. Yang, M. Ren, and B. Xu, "Retinal blood vessel segmentation with improved convolutional neural networks," *Journal of Medical Imaging and Health Informatics*, vol. 9, no. 6, pp. 1112–1118, 2019.
- [14] S. Guo, K. Wang, H. Kang, Y. Zhang, Y. Gao, and T. Li, "Bts-dsn: Deeply supervised neural network with short connections for retinal vessel segmentation," *International journal of medical informatics*, vol. 126, pp. 105–113, 2019.
- [15] A. Hatamizadeh, H. Hosseini, Z. Liu, S. D. Schwartz, and D. Terzopoulos, "Deep dilated convolutional nets for the automatic segmentation of retinal vessels," *arXiv preprint arXiv:1905.12120*, 2019.
- [16] Z. Fan, J. Mo, and B. Qiu, "Accurate retinal vessel segmentation via octave convolution neural network," *arXiv preprint arXiv:1906.12193*, 2019.
- [17] K. J. Noh, S. J. Park, and S. Lee, "Scale-space approximated convolutional neural networks for retinal vessel segmentation," *Computer methods and programs in biomedicine*, vol. 178, pp. 237–246, 2019.
- [18] Q. Jin, Q. Chen, Z. Meng, B. Wang, and R. Su, "Construction of retinal vessel segmentation models based on convolutional neural network," *Neural Processing Letters*, pp. 1–18, 2019.
- [19] J. Li, "An empirical comparison between svms and anns for speech recognition," in *The First Instructional Conf. on Machine Learning*, vol.951, 2003, p. 2003.
- [20] E. Reinhard, M. Adhikhmin, B. Gooch, and P. Shirley, "Color transfer between images," *IEEE Computer graphics and applications*, vol. 21, no. 5, pp. 34–41, 2001.
- [21] W. Kusakunniran, A. Wiratsudakul, U. Chuachan, S. Kanchanapreechakorn, and T. Imaromkul, "Automatic cattle identification based on fusion of texture features extracted from muzzle images," in *2018 IEEE International Conference on Industrial Technology (ICIT).*, IEEE, 2018, pp. 1484–1489.
- [22] D. Barina, "Gabor wavelets in image processing," *arXiv preprint arXiv:1602.03308*, 2016.
- [23] M. M. Fraz, P. Remagnino, A. Hoppe, S. Velastin, B. Uyyanonvara, and S. Barman, "A supervised method for retinal blood vessel segmentation using line strength, multiscale gabor and morphological features," in *Signal and Image Processing Applications (ICSIPA), 2011 IEEE International Conference on.*, IEEE, 2011, pp. 410–415.
- [24] I. Steinwart and A. Christmann, *Support vector machines.*, Springer Science & Business Media, 2008.
- [25] A. Iranmehr, H. Masnadi-Shirazi, and N. Vasconcelos, "Cost-sensitive support vector machines," *Neurocomputing*, 2019.
- [26] W. Kusakunniran, K. Ngamascharyakul, C. Chantaraviwat, K. Janvittayanuchit, and K. Thongkanchorn, "A Thai license plate localization using svm," in *2014 International Computer Science and Engineering Conference (ICSEC).*, IEEE, 2014, pp. 163–167.
- [27] P. Druzhkov, V. Erukhimov, N. Y. Zolotykh, E. Kozinov, V. Kustikova, I. Meerov, and A. Polovinkin, "New object detection features in the opencv library," *Pattern Recognition and Image Analysis*, vol. 21, no. 3, p. 384, 2011.
- [28] C.-C. Chang and C.-J. Lin, "Libsvm: A library for support vector machines," *ACM transactions on intelligent systems and technology (TIST)*, vol. 2, no. 3, p. 27, 2011.
- [29] G. Bradski and A. Kaehler, *Learning OpenCV: Computer vision with the OpenCV library.*, "O'Reilly Media, Inc.", 2008.
- [30] P. K. Ghosh and R. M. Haralick, "Mathematical morphological operations of boundary repre-

- sented geometric objects," *Journal of Mathematical Imaging and Vision*, vol. 6, no. 2-3, pp. 199–222, 1996.
- [31] J. B. Roerdink and A. Meijster, "The watershed transform: Definitions, algorithms and parallelization strategies," *Fundamenta informaticae*, vol. 41, no. 1, 2, pp. 187–228, 2000.
- [32] C. Rother, V. Kolmogorov, and A. Blake, "Grabcut: Interactive foreground extraction using iterated graph cuts," in *ACM transactions on graphics (TOG)*, vol. 23, no. 3. ACM, 2004, pp. 309–314.
- [33] M. Eapen, R. Korah, and G. Geetha, "Swarm intelligence integrated graph-cut for liver segmentation from 3d-ct volumes," *The Scientific World Journal*, vol. 2015, 2015.
- [34] L. Massoptier and S. Casciari, "Fully automatic liver segmentation through graph-cut technique," in *2007 29th Annual International Conference of the IEEE Engineering in Medicine and Biology Society.*, IEEE, 2007, pp. 5243–5246.
- [35] J. Cha, M. M. Farhangi, N. Dunlap, and A. A. Amini, "Segmentation and tracking of lung nodules via graph-cuts incorporating shape prior and motion from 4d ct," *Medical physics*, vol. 45, no. 1, pp. 297–306, 2018.
- [36] J. won Cha, N. Dunlap, B. Wang, and A. Amini, "3d segmentation of lung ct data with graph-cuts: analysis of parameter sensitivities," in *Medical Imaging 2016: Biomedical Applications in Molecular, Structural, and Functional Imaging*, vol. 9788. International Society for Optics and Photonics, 2016, p. 97882O.
- [37] J. F. Talbot and X. Xu, "Implementing grabcut," Brigham Young University, vol. 3, 2006.
- [38] T. Malmer, "Image segmentation using grabcut," *IEEE Transactions on Signal Processing*, vol. 5, no. 1, pp. 1–7, 2010.
- [39] A. Blake, C. Rother, M. Brown, P. Perez, and P. Torr, "Interactive image segmentation using an adaptive gmmrf model," in *European conference on computer vision.*, Springer, 2004, pp.428–441.
- [40] Y. Boykov and V. Kolmogorov, "An experimental comparison of min-cut/max-flow algorithms for energy minimization in vision," *IEEE Transactions on Pattern Analysis & Machine Intelligence*, no. 9, pp. 1124–1137, 2004.
- [41] M. Stoer and F. Wagner, "A simple min-cut algorithm," *Journal of the ACM (JACM)*, vol. 44, no. 4, pp. 585–591, 1997.
- [42] A. Hoover and M. Goldbaum, "Locating the optic nerve in a retinal image using the fuzzy convergence of the blood vessels," *IEEE transactions on medical imaging*, vol. 22, no. 8, pp. 951–958, 2003.
- [43] C. Wang, Z. Zhao, Q. Ren, Y. Xu, and Y. Yu, "Dense u-net based on patch-based learning for retinal vessel segmentation," *Entropy*, vol. 21, no. 2, p. 168, 2019.
- [44] B. Zupan, E. T. Keravnou, and N. Lavrac, *Intelligent Data Analysis in Medicine and Pharmacology*. Kluwer Academic Publishers, 1997.



Worapan Kusakunniran received the B.Eng. degree in computer engineering from the University of New South Wales (UNSW), Sydney, Australia, in 2008, and the Ph.D. degree in computer science and engineering from UNSW, in cooperation with the Neville Roach Laboratory, National ICT Australia, Kensington, Australia, in 2013. He is currently a Lecturer with the Faculty of Information and Communication Technology, Mahidol University, Nakhon Pathom, Thailand. He is the author of several papers in top international conferences and journals. His current research interests include biometrics, pattern recognition, medical image processing, computer vision, multimedia, and machine learning.

Dr. Kusakunniran served as a Program Committee Member for many international conferences and workshops. Also, he has served as a Reviewer for several international conferences and journals, such as the International Conference on Pattern Recognition, the IEEE International Conference on Image Processing, the IEEE International Conference on Advanced Video and Signal based Surveillance, the Pattern Recognition, the IEEE TRANSACTIONS ON SYSTEMS, MAN, AND CYBERNETICS, PART B: CYBERNETICS, the IEEE TRANSACTIONS ON IMAGE PROCESSING, the IEEE TRANSACTIONS ON INFORMATION FORENSICS AND SECURITY, and the IEEE SIGNAL PROCESSING LETTERS. He was a recipient of the ICPR Best Biometric Student Paper Award in 2010, and also a winner of several national and international innovation contests.



Peeraphat Charoenpanich received the B.Sc. degree in information and communication technology from Faculty of Information and Communication Technology, Mahidol University, Nakhon Pathom, Thailand. He is currently an IT Consultant with Revenue Department, Thailand. His current research interests include pattern recognition and computer vision.



Perapat Samunyanoraset received the B.Sc. degree in information and communication technology from Faculty of Information and Communication Technology, Mahidol University, Nakhon Pathom, Thailand. He is currently pursuing the M.Sc. degree in Computing from University of Northampton, United Kingdom. His current research interests include pattern recognition and computer vision.



Sarocha Suksai received the B.Sc. degree in information and communication technology from Faculty of Information and Communication Technology, Mahidol University, Nakhon Pathom, Thailand. She is currently a Software Analyst with Mass Rapid Transit Authority of Thailand. Her current research interests include pattern recognition and computer vision.



Sarattha Karnjanapreechakorn received the B. Eng. degree in Electrical-Mechanical Manufacturing Engineering from Kasetsart University, Bangkok, Thailand in 2015, and M.Sc. degree in Information and Communication Technology from University of Mahidol, Nakhon Pathom, Thailand 2017. He is currently a machine learning developer and data scientist. His current research is in the deep learning field.



Qiang Wu received the B.Eng. and M.Eng. degrees from the Harbin Institute of Technology, Harbin, China, in 1996 and 1998, respectively, and the Ph.D. degree from the University of Technology Sydney, Australia, in 2004. He is currently an Associate Professor and a Core Member of the Global Big Data Technologies Centre, University of Technology Sydney. His research interests include computer

vision, image processing, pattern recognition, machine learning, and multimedia processing. The application fields where the research outcomes are applied span over video security surveillance, biometrics, video data analysis, and human-computer interaction. His research outcomes have been published in many premier international conferences, including ECCV, CVPR, ICCV, ICIP, and ICPR and the major international journals, such as the IEEE TIP, IEEE TSMC-B, IEEE TCSVT, IEEE TIFS, PR, PRL, and Signal Processing.



Jian Zhang received the B.S. degree in electronics from East China Normal University, China, the M.S. degree in computer science from Flinders University, Australia, and the Ph.D. degree in electrical engineering from University of New South Wales (UNSW), Australia. From 1997 to 2003, he was with the Visual Information Processing Laboratory, Motorola Labs, Sydney, as a Principal Research Engineer and the Research

Manager of visual communications. From 2004 to 2011, he was a Principal Researcher and a Project Leader with Data61 (formerly INCTA), Australia, and a Conjoint Associate Professor with the School of Computer Science and Engineering, UNSW.

He is currently an Associate Professor with the Global Big Data Technologies Centre, School of Electrical and Data Engineering, Faculty of Engineering and Information Technology, University of Technology Sydney, Australia. He is the author or co-author of more than 140 paper publications and book chapters and holds six issued U.S. and Chinese patents. His current interests include social multimedia signal processing, large-scale image and video content analytics, retrieval and mining, 3D-based computer vision, and intelligent video surveillance systems.

Dr. Zhang was the General Co-Chair of the International Conference on Multimedia and Expo in 2012 and the Technical Program Co-Chair of the IEEE Visual Communications and Image Processing in 2014. He was an Associate Editor of IEEE TRANSACTIONS ON CIRCUITS AND SYSTEMS FOR VIDEO TECHNOLOGY from 2006 to 2015. He has been an Associate Editor for IEEE TRANSACTIONS ON MULTIMEDIA and EURASIP Journal on Image and Video Processing since 2016.